



A two-step thermal annealing and HNO₃ doping treatment for graphene electrode and its application in small-molecule organic solar cells



Yang Chen^a, Jing Feng^{a,*}, Feng-Xi Dong^a, Yun-Fei Li^a, Yan-Gang Bi^a, Yuan-Yuan Yue^a, Hong-Bo Sun^{a,b}

^a State Key Laboratory on Integrated Optoelectronics, College of Electronic Science and Engineering, Jilin University, 2699 Qianjin Street, Changchun 130012, People's Republic of China

^b College of Physics, Jilin University, 119 Jiefang Road, Changchun 130023, People's Republic of China

ARTICLE INFO

Article history:

Received 20 July 2016

Accepted 24 July 2016

Keywords:

Graphene

Thermal annealing

Doping treatment

Small-molecule organic solar cells

ABSTRACT

The transferred chemical vapor deposition (CVD)-grown graphene from copper foils to other desired substrates by using poly(methyl methacrylate) (PMMA) as supporter, suffers from problems of rough surface, low conductivity and poor wettability, which hinders its applications in optoelectronic devices. In this work, a combined thermal annealing and HNO₃ doping treatment for graphene electrode has been employed to simultaneously improve its smoothness, conductivity and wettability. The thermal annealing process results in the improved surface smoothness by removing the PMMA residue. HNO₃ doping treatment for the graphene enhances its conductivity and surface wetting to PEDOT:PSS. Furthermore, the work function (WF) of two-step treated graphene increased from ~4.4 eV to ~5.1 eV. Small-molecule organic solar cells (OSCs) based on the two-step treated graphene anodes exhibit a power conversion efficiency (PCE) of 2.43%, which is comparable to that of ITO electrode (2.48%). This work demonstrates the bright future of graphene transparent electrodes as a replacement for ITO.

© 2016 Elsevier B.V. All rights reserved.

1. Introduction

Organic solar cells (OSCs) have gained much attention as the next generation of clean electricity due to its fascinating properties such as light weight, low cost, large-area processes and flexibility [1–5]. Indium tin oxide (ITO) is generally used as a transparent conducting electrode (TCE) in optoelectronics [6–8]. However, the intrinsic sensitivity to acid and heat has restricted its use in some special area, beyond that, the limited storage of indium on earth and mechanical brittleness of ITO would further limit its application in tomorrow OSCs [9–11]. Graphene grown by chemical vapor deposition (CVD) has shown dramatic advances in the past several decades, offering many remarkable advantages including high transparency, mechanical stability and ultrahigh carrier mobility [12–14]. Monolayer graphene is a one-atom thick planar sheet

consist of carbon atoms forming by hexagonal arrangement, which has been widely used as TCEs in optoelectronics, such as circuits [15], organic light-emitting diodes (OLEDs) [16] and OSCs [12,13], emerged as a promising material choice for a potential alternative to commonly used ITO as a TCE.

However, the further application of graphene usually requires a wet transfer process from grown Copper foils to other desired substrates through a PMMA supporting layer, which could induce obvious PMMA residue on its surface though after a treatment with hot acetone (here named “as-transferred graphene”) [17,18]. The PMMA residue results in a rough surface of the graphene, a mass of protuberances on electrode surface would significantly decrease their performance, due to a high leak current or even breakdown [19–21]. In this way, it seems reasonable that graphene is broadly used in bulk polymer OSCs rather than small molecule-based OSCs for the prior's lower request of surface roughness [22–24]. In order to decrease the surface roughness caused by the PMMA residue, a quite long heating period (usually several hours) in acetone is required to get a smooth graphene surface [25]. Jens et al. also mentioned a thermal annealing process in H₂ to further remove the

* Corresponding author. State Key Laboratory on Integrated Optoelectronics, College of Electronic Science and Engineering, Jilin University, 2699 Qianjin Street, Changchun 130012, People's Republic of China.

E-mail address: jingfeng@jlu.edu.cn (J. Feng).

polymer, but particular research on its effect process was not carried out [26]. In addition, as-transferred monolayer graphene always suffers from the challenge of relatively high sheet resistance (R_s) and poor surface wetting to hole-transporting layer. Most of the as-transferred monolayer graphene film reported in the previous literature has shown a high R_s of $\sim 1 \text{ k}\Omega/\square$ or even higher [20,27–29]. Furthermore, the work function (WF) of as-transfer graphene is usually around 4.4 eV, which is mismatched with the energy level of hole-transporting layer, and hinders the carrier injection or extraction in the optoelectronic devices used as its electrodes [13,30,31].

Here, we demonstrate a two-step treatment method of the transferred CVD-grown graphene from the Cu foil to the desired substrate by combining thermal annealing and HNO_3 doping treatment to improve its properties and apply it as electrode in OSCs. The thermal annealing process in CVD furnace under H_2 flow for graphene after a hot acetone treatment significantly improves its surface morphology. A large range of disposed temperature (200–500 °C) and the corresponding characteristics of graphene are discussed in detail. As the temperature increasing, the G band position of graphene Raman spectra shows a blue-shift from 1577 cm^{-1} to 1598 cm^{-1} , consistent with an increased p-type doped effect. HNO_3 were used as a dopant to further enhance graphene's conductivity and surface wetting to PEDOT:PSS. R_s value for the two-step treated graphene is $\sim 400\text{--}500 \Omega/\square$, which is twofold less than as-transferred graphene. Moreover, the WF of the two-step treated graphene is 0.7 eV increased, which is benefit to the carrier collection in the OSCs. The small molecule-based OSCs with the two-step treated graphene electrodes exhibit a comparable PCE to that of the devices based on ITO electrode.

2. Experimental methods

2.1. Growth, transfer and treatment of the monolayer graphene

Large area ($2 \times 1.8 \text{ cm}^2$) monolayer graphene is synthesized via low pressure CVD (LPCVD) on 25 μm thick copper foils (Alfa Aesar, 7440-50-8) is shown in Fig. 1a, with 5 sccm CH_4 , 10 sccm H_2 and 100 sccm Ar flowing during growth at a growth temperature of 1060 °C for 30 min. PMMA-supported graphene wet transfer process is shown in Fig. 1b–g. 5% wt PMMA (Aladdin, 9011-14-7) dissolved in anisole is spin-coated on one side of the graphene on copper foils with a thickness of $\sim 300 \text{ nm}$ for graphene protection, and the other side is treated with Ar plasma for 5 min to destroy the structure of this side's graphene. 0.5 M FeCl_3 solution is used for copper etching, leaving the PMMA-graphene membrane floats on the solution after approximately 5 h, then the membrane is transferred to glass or Si/SiO₂ substrates. PMMA first removed in 80 °C acetone for 30 min, followed by a alcohol and DI water washing. In order to further remove the PMMA residue, graphene is thermally annealed in a LPCVD furnace with 50 sccm H_2 for 1 h (Fig. 1h), a large range of temperature is employed, from 200 °C to 500 °C. The doping treatment is shown in Fig. 1i, 5% vol HNO_3 in DI water is first drop on graphene surface for a full coverage, then maintains for 2 min to realize the doping process, finally a spin-coated step at 3000 r is applied to throw off the dopant, repeat this section once again for exhaustive dope of graphene.

The morphologies of the monolayer graphene have been detected by atomic force microscopy (AFM, Dimension Icon, Bruker Corporation) in tapping mode. Raman spectra of graphene measured by Raman Spectrometer (LabRAM HR Evolution, HORIBA) with a laser excitation energy of 532 nm. UV-Vis spectrophotometer (UV-2550, SHIMADZU) and four point probe tester are used to measure the transmittance/absorption spectra and

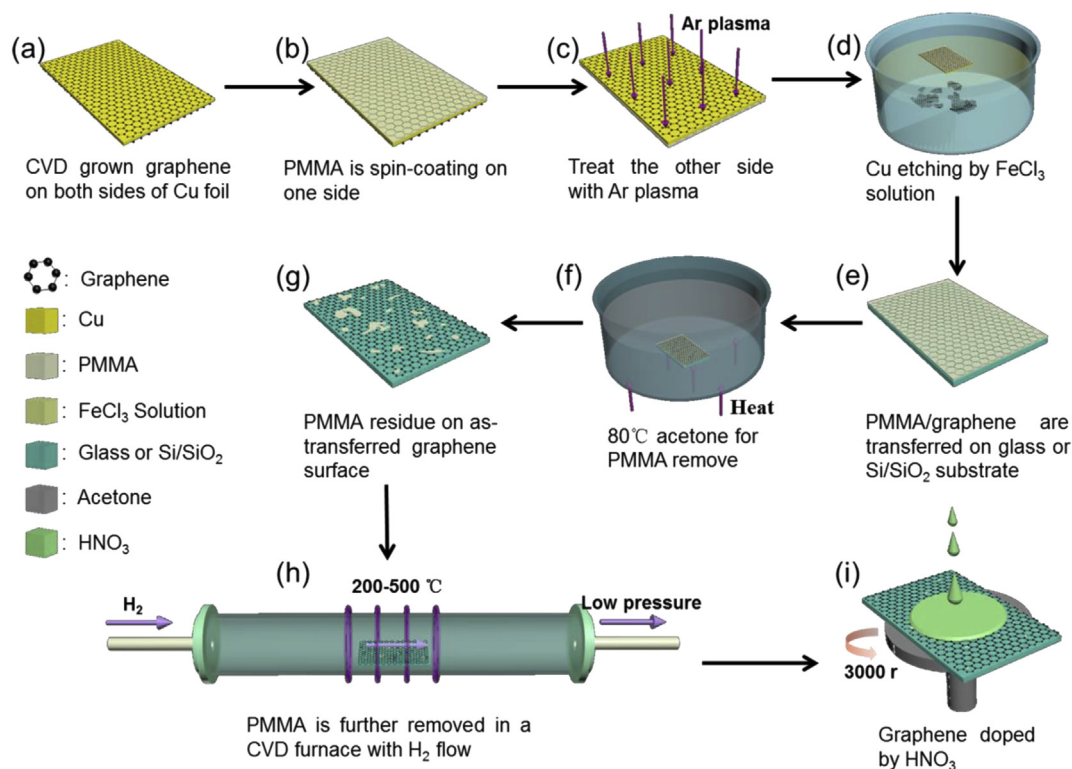


Fig. 1. (a)–(g) Schematic of the wet transfer process for the PMMA-supported graphene. (h) An added thermal annealing process to further clean the graphene surface in a CVD furnace. (i) HNO_3 doping treatment for annealed graphene by a spin coater.

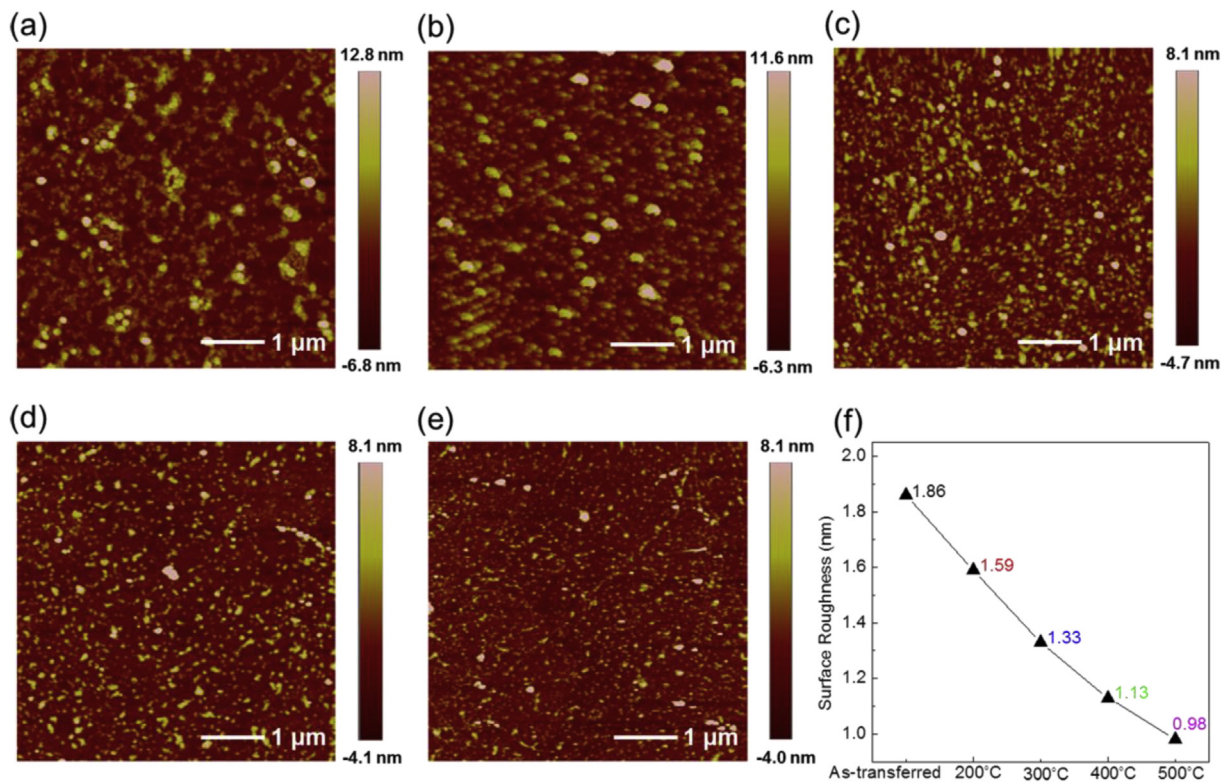


Fig. 2. AFM images of as-transferred graphene (a), 200 °C annealed graphene (b), 300 °C annealed graphene (c), 400 °C annealed graphene (d) and 500 °C annealed graphene (e). (f) The corresponding graphene rms surface roughness (R_a) variation in (a)–(e).

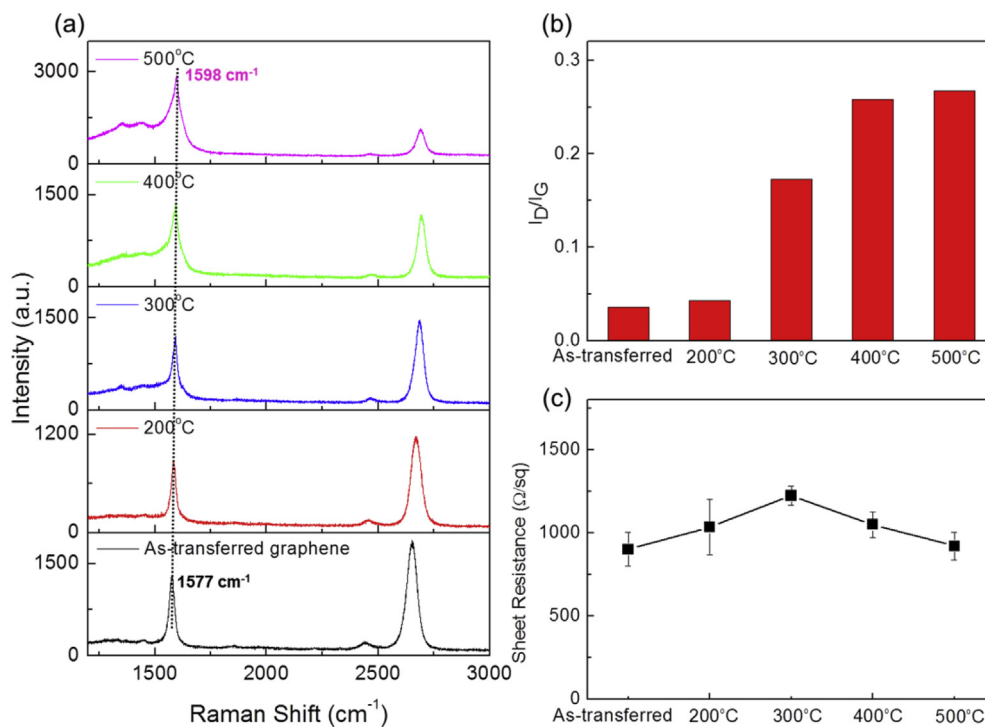


Fig. 3. (a) Raman spectra of as-transferred graphene and different temperatures annealed graphene, a dash line shows blue-shift of G bands as temperature rising. (b) Histogram distributions of I_D/I_G intensity ratio extracted from Raman spectra data in Fig. 3(a). (c) Sheet resistance variation of as-transferred graphene and different temperatures annealed graphene. (For interpretation of the references to color in this figure legend, the reader is referred to the web version of this article.)

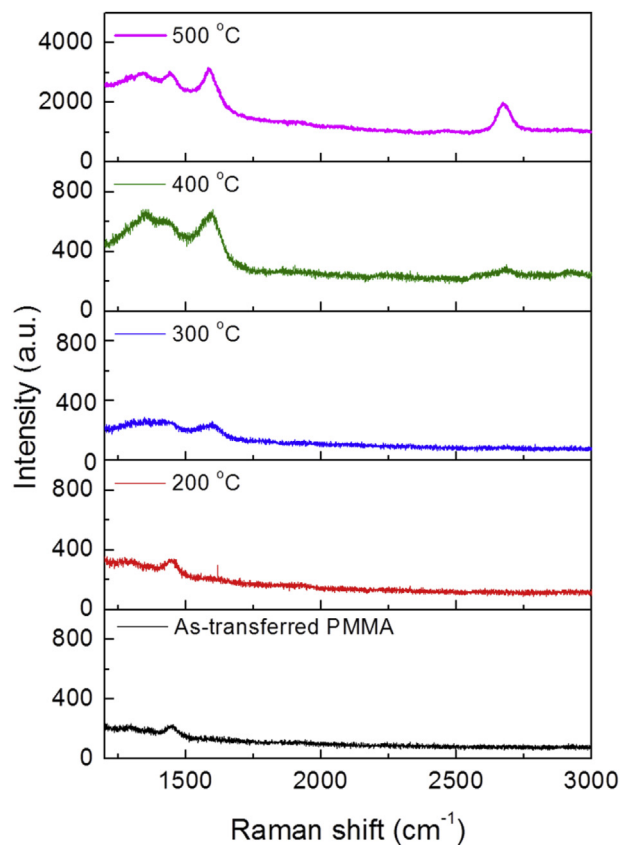


Fig. 4. Raman spectra of as-transferred PMMA and “PMMA-converted material” at different annealed temperatures, the condition is identical as described in Fig. 1 except on Copper foils without graphene grown.

sheet resistance, respectively.

2.2. Fabrication and evaluation of the small-molecule OSCs

For small-molecule OSCs fabrication, PEDOT:PSS is firstly spin-coated (3000 r 1 min) on graphene as a smoothing and hole-transporting layer, then a 5 nm MoO₃, 15 nm boron subphthalocyanine chloride (SubPc), 40 nm fullerene (C₆₀), 3 nm bathocuproine (BCP), and Ca (2 nm)/Ag (80 nm) are evaporated sequentially in a thermal evaporation chamber at a base pressure of 5×10^{-4} Pa. The device performance of solar cells is measured by a sourcemeter (Keithley 2400) under 1 sun simulated AM 1.5 G illumination (100 mW/cm²).

3. Results and discussion

As for surface morphology of graphene electrode, PMMA merely disposed with hot acetone for a relatively short possible time remains abundant PMMA residue. As can be observed in the AFM image shown in Fig. 2a, PMMA residue are very strongly adhered to as-transferred graphene surface with numerous “island” higher than 10 nm. In order to remove the PMMA residue, graphene is further annealed in a LPCVD furnace with different temperatures. H₂ plays the part of protection gas and constructs reducing atmosphere. Considering the melting point of PMMA (130–140 °C), 200, 300, 400, 500 °C have been examined, corresponding AFM images are shown in Fig. 2b–e, respectively. With a thermal annealing process, PMMA melt into nanoparticle-like states. As the temperature rising, both the density and size of “nanoparticles”

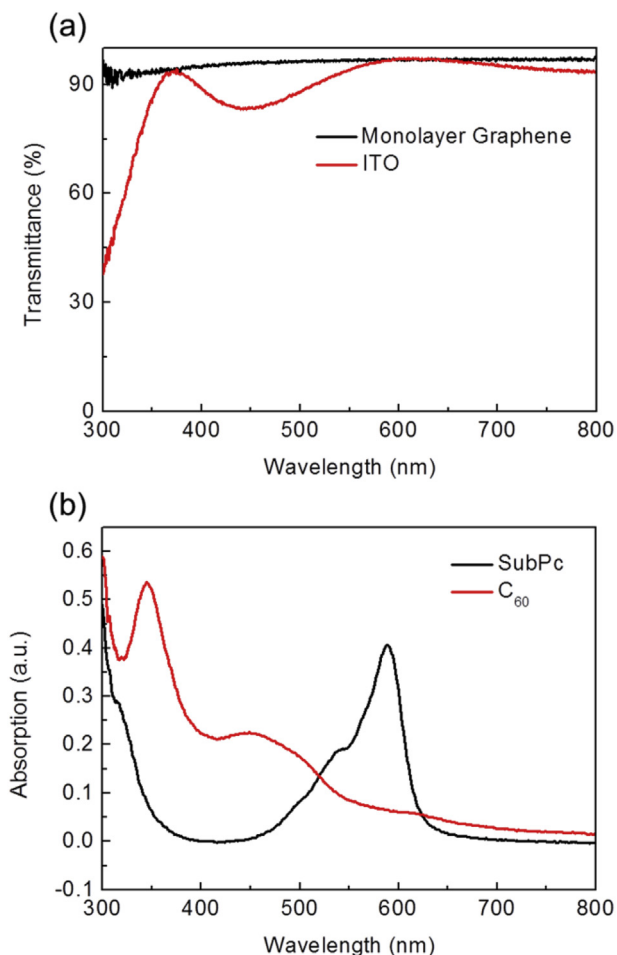


Fig. 5. (a) Transmission spectrum of the monolayer graphene and ITO. (b) Absorption spectra of the SubPc and C₆₀ films.

decreasing because of the “burn effect” to PMMA, confirming smoother graphene morphology is obtained. Fig. 2f shows graphene root-mean-square (rms) surface roughness (Ra), which is changed with different annealing temperatures. The Ra at annealing temperature of 500 °C is 0.98 nm, which reduces to about half of that without thermal annealing process (1.86 nm).

We investigate the Raman spectra of the monolayer graphene on Si/SiO₂ substrates before and after thermal annealing treatment, as shown in Fig. 3a. The G band and 2D band of as-transferred graphene are located at 1577 cm⁻¹ and 2654 cm⁻¹ with I_{2D}/I_G ~2, verifying its monolayer nature. It is noted that no discernible defect-related D band is observed, and it is clearly indicative of the high quality of the samples [13,32]. After thermal annealing process, the G band position shows a blue-shift from 1577 cm⁻¹ to 1598 cm⁻¹ as the temperature increasing. Assuming that $\Delta\Omega_G = \Delta E_F \times 42 \text{ cm}^{-1} \text{ eV}^{-1}$, where $\Delta\Omega_G$ is the G peak shift and ΔE_F is the Fermi level shift, the WF of as-transferred graphene and 500 °C annealed graphene are measured to be 4.4 and 4.9 eV, which shows a strong p-type doping effect [33,34]. Fig. 3b shows the corresponding relative changes in the I_D/I_G ratio after graphene disposed with different temperatures. The I_D/I_G ratio is less than 0.05 for the as-transferred graphene. As the temperature is equal or higher than 300 °C, detectable D band around 1351 cm⁻¹ is found in Fig. 3a, and the corresponding I_D/I_G ratio is ~0.2. It seems like high temperature would cause obvious defect to graphene, however, sheet resistance of monolayer graphene maintains around 1 kΩ/□ in all conditions,

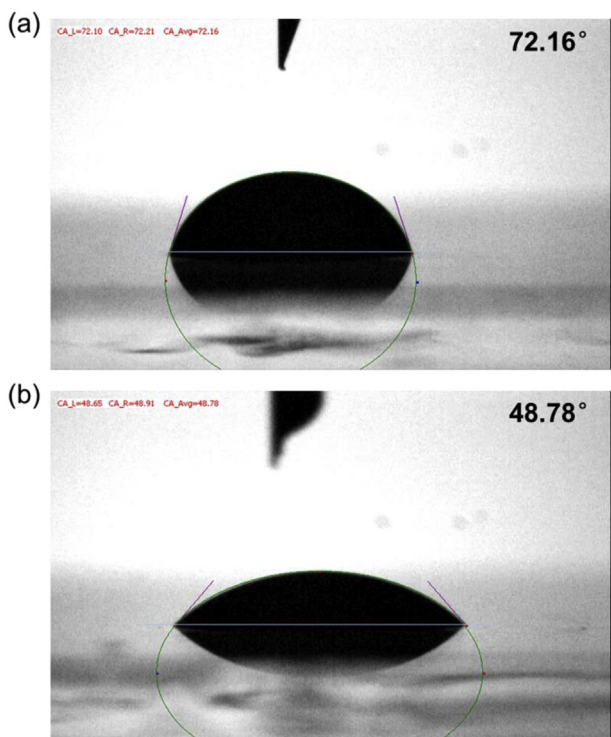


Fig. 6. PEDOT:PSS–500 °C annealed graphene contact angles before (a) and after (b) HNO₃ doping.

as can be seen in Fig. 3c. We consider the contradictory phenomenon might have a potential mechanism under its cover.

Li et al. have reported that PMMA as carbon source for graphene grown at a relative low temperature [35]. Considering this, contrast experiment under identical conditions as described in Fig. 1 is carried out on Copper foils without graphene grown, corresponding Raman spectra of “PMMA-converted material” is shown in Fig. 4. As-transferred PMMA without a thermal annealing process shows a Raman signal peak around 1446 cm⁻¹, which is supposed to belong to PMMA. As the temperature reaching to 300 °C, dumpy D and G band are discovered around 1356 cm⁻¹ and 1586 cm⁻¹. Further increasing the temperature to 400 °C, relatively sharp D and G band appears accompany with a weak 2D band. When the

temperature is increased to 500 °C, graphene-like Raman spectra with significant D, G and 2D band is obtained, confirming graphene formed from PMMA. Therefore, the D band shown in Fig. 3a might come from “PMMA-converted material”, additionally has effect to dwarf the intensity of 2D band compared to G band at the temperature of 400 and 500 °C, which is consistent with an increase in p-type doping for graphene after an annealing process [36–38].

The transmittance of the monolayer graphene and ITO are compared in Fig. 5a, the prior has ~97% transmittance in the visible region, higher than ITO in some certain wavelength, which has been confirmed in previous research [19,34]. To further improve the conductivity and surface wetting of annealed graphene, HNO₃ is chosen as the chemical dopant because it is an effective approach to tailor the electronic properties of graphene films. After doping, the sheet resistance of the two-step treated graphene is reduced by approximately one half to ~400–500 Ω/□ compared with 500 °C annealed graphene. The PEDOT:PSS–graphene contact angles before and after doping is investigated in Fig. 6. The contact angle of the 500 °C annealed graphene is calculated to be 72.16°, while it is 48.78° for the two-step treated graphene, indicating an improved graphene surface wetting to PEDOT:PSS. We believe that improved surface wetting of graphene is beneficial to form smooth and tight PEDOT:PSS films, which would further enhance the performance of our device.

The small-molecule OSCs device structure and energy level distribution schematic diagrams are shown in Fig. 7. The WF of the two-step treated graphene is measured to be 5.1 eV with Kelvin Probe, higher than 4.9 eV of 500 °C annealed graphene, which is well matched with HOMO level of PEDOT:PSS (5.2 eV). The performance of small-molecule OSCs devices with different conditions are compared in Fig. 8 and the detail photovoltaic parameters are list in Table 1. For graphene-based small-molecule OSCs, the PCE shows obvious enhancement as the annealed temperature grows up, which originates from the improvement of fill factors (FF) mainly connected with surface roughness. The FF for as-transferred graphene-based device is 33.97%, and it is increased to 46.34% for the 500 °C annealed graphene-based device, which corresponds to an enhances PCE from 1.59% to 2.24%. The two-step treated graphene-based device exhibits a higher FF up to 50.90%, which might attribute to the lower interface resistance and matched energy level, as well as a smoother PEDOT:PSS layer. Comparing with the ITO, graphene has higher transmittance in some certain wavelength which is beneficial for increasing the active layers' absorption, as shown in Fig. 5b. As a result, the short-circuit current

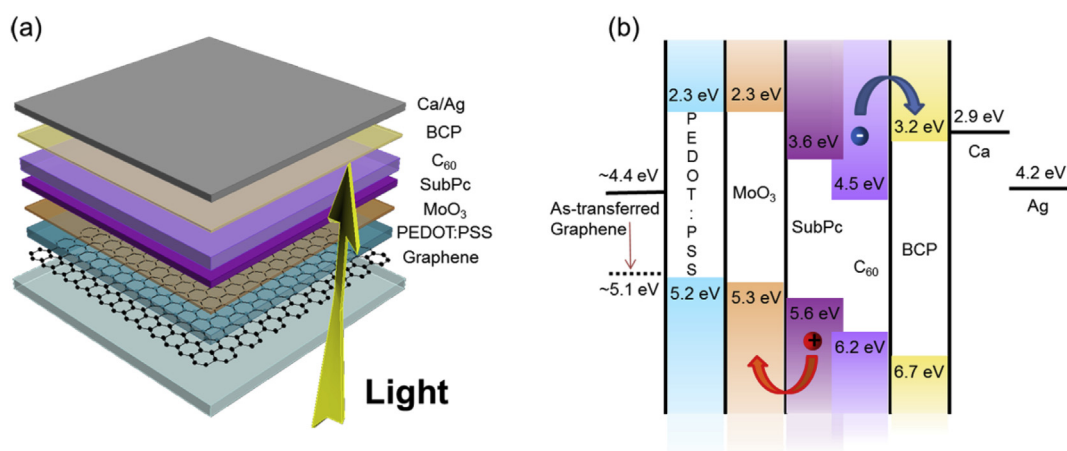


Fig. 7. (a) Schematic diagram of photovoltaic device structure. (b) Energy level distribution diagram of the small-molecule OSCs. With 500 °C thermal annealing and HNO₃ doping treatment, the WF of as-transferred graphene increased from ~4.4 eV to ~5.1 eV.

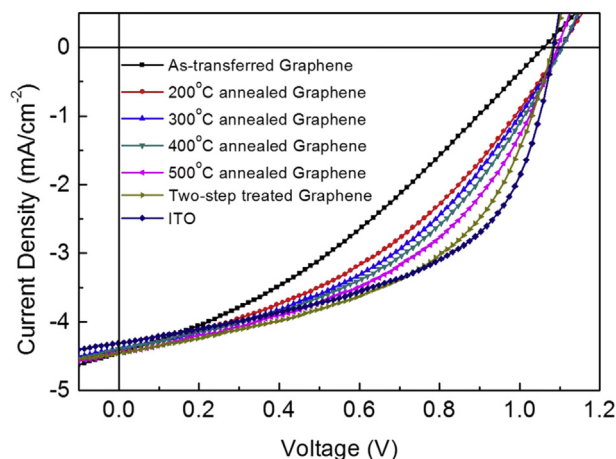


Fig. 8. Current density-voltage characteristics of small-molecule OSCs with different conditions treated graphene electrodes and ITO electrode.

Table 1

A summary of photovoltaic performance parameters of small-molecule OSCs investigated in this work.

	Voc [V]	Jsc [mA/cm ²]	FF [%]	PCE [%]
As-transferred graphene	1.06	4.43	33.97	1.59
200 °C annealed graphene	1.10	4.39	40.41	1.95
300 °C annealed graphene	1.10	4.37	42.85	2.06
400 °C annealed graphene	1.10	4.39	44.28	2.14
500 °C annealed graphene	1.09	4.45	46.34	2.24
Two-step treated graphene	1.07	4.45	50.90	2.43
ITO	1.07	4.30	53.86	2.48

density (J_{sc}) has been improved from 4.30 mA/cm² to 4.45 mA/cm², small-molecule OSCs based on 500 °C anneal-doped graphene obtains a PCE of 2.43%, comparable to that of ITO electrode (2.48%). These results demonstrate that the two-step thermal annealing and HNO₃ doping treatment for graphene is potential electrodes for efficient small-molecule OSCs.

4. Conclusions

In summary, we have demonstrated a two-step treatment method of the transferred CVD-grown graphene from Cu foil to the desired substrate by combining thermal annealing and doping treatment to simultaneously improve its smoothness, conductivity and wettability. The PMMA residue has been removed by the thermal annealing treatment to obtain a smoother graphene surface. Combined with chemically doping treatment, the conductivity and the surface wetting to PEDOT:PSS is significantly improved. Moreover, the WF of two-step treated graphene further shifts to 5.1 eV, which is well matched with the energy level of PEDOT:PSS. Small-molecule OSCs based on the two-step treated graphene shows a PCE of 2.43%, which is comparable with ITO-based device, further confirming the two-step treatment for graphene electrodes has an obviously beneficial effect for graphene-based device.

Acknowledgements

The authors gratefully acknowledge the support from the 973 and NSFC programs under Grant Nos. 61322402, 61590930, 2013CBA01700, 51373064 and 61505065.

References

- [1] R. Sharma, S. Bhalariao, D. Gupta, Effect of incorporation of CdS NPs on performance of PTB7: PCBM organic solar cells, *Org. Electron* 33 (2016) 274–280.
- [2] X.X. Yin, Q.S. An, J.S. Yu, F.N. Guo, Y.L. Geng, L.Y. Bian, Z.S. Xu, B.J. Zhou, L.H. Xie, F.J. Zhang, W.H. Tang, Side-chain engineering of benzo[1,2-b:4,5-b']dithiophene core-structured small molecules for high-performance organic solar cells, *Sci. Rep.* 6 (2016).
- [3] J. Kim, G. Kim, H. Back, J. Kong, I.W. Hwang, T.K. Kim, S. Kwon, J.H. Lee, J. Lee, K. Yu, C.L. Lee, H. Kang, K. Lee, High-performance integrated perovskite and organic solar cells with enhanced fill factors and near-infrared harvesting, *Adv. Mater.* 28 (2016) 3159–3165.
- [4] Y. Gu, C. Wang, T.P. Russell, Multi-length-scale morphologies in PCPDTBT/PCBM bulk-heterojunction solar cells, *Adv. Energy Mater.* 2 (2012) 683–690.
- [5] J.B. You, L.T. Dou, K. Yoshimura, T. Kato, K. Ohya, T. Moriarty, K. Emery, C.C. Chen, J. Gao, G. Li, Y. Yang, A polymer tandem solar cell with 10.6% power conversion efficiency, *Nat. Commun.* 4 (2013).
- [6] S.H. Park, S.J. Lee, J.H. Lee, J. Kal, J. Hahn, H.K. Kim, Large area roll-to-roll sputtering of transparent ITO/Ag/ITO cathodes for flexible inverted organic solar cell modules, *Org. Electron* 30 (2016) 112–121.
- [7] S. Chang, G.D. Han, J.G. Weis, H. Park, O. Hentz, Z.B. Zhao, T.M. Swager, S. Gradecak, Transition metal-oxide free perovskite solar cells enabled by a new organic charge transport layer, *ACS Appl. Mater. Interfaces* 8 (2016) 8511–8519.
- [8] J.Y. Kim, K. Lee, N.E. Coates, D. Moses, T.Q. Nguyen, M. Dante, A.J. Heeger, Efficient tandem polymer solar cells fabricated by all-solution processing, *Science* 317 (2007) 222–225.
- [9] I. Jeon, K. Cui, T. Chiba, A. Anisimov, A.G. Nasibulin, E.I. Kauppinen, S. Maruyama, Y. Matsuo, Direct and dry deposited single-walled carbon nanotube films doped with MoO_x as electron-blocking transparent electrodes for flexible organic solar cells, *J. Am. Chem. Soc.* 137 (2015) 7982–7985.
- [10] X.T. Hu, L. Chen, L.C. Tan, T. Ji, Y. Zhang, L. Zhang, D. Zhang, Y.W. Chen, In situ polymerization of ethylenedioxythiophene from sulfonated carbon nanotube templates: toward high efficiency ITO-free solar cells, *J. Mater. Chem. A* 4 (2016) 6645–6652.
- [11] G.A. dos R. Benatto, B. Roth, M. Corazza, R.R. Søndergaard, S.A. Gevorgyan, M. Jørgensen, F.C. Krebs, Roll-to-roll printed silver nanowires for increased stability of flexible ITO-free organic solar cell modules, *Nanoscale* 8 (2016) 318–326.
- [12] H. Sung, N. Ahn, M.S. Jang, J.K. Lee, H. Yoon, N.G. Park, M. Choi, Transparent conductive oxide-free graphene-based perovskite solar cells with over 17% efficiency, *Adv. Energy Mater.* 6 (2016).
- [13] Z.K. Liu, P. You, S.H. Liu, F. Yan, Neutral-color semitransparent organic solar cells with all-graphene electrodes, *ACS Nano* 9 (2015) 12026–12034.
- [14] Y.P. Hsieh, C.L. Kuoa, M. Hofmann, Ultrahigh mobility in polyolefin-supported graphene, *Nanoscale* 8 (2016) 1327–1331.
- [15] T.H. Bointon, G.F. Jones, A.D. Sanctis, R. Hill-Pearce, M.F. Craciun, S. Russo, Large-area functionalized CVD graphene for work function matched transparent electrodes, *Sci. Rep.* 5 (2015).
- [16] T.H. Han, Y. Lee, M.R. Choi, S.H. Woo, S.H. Bae, B.H. Hong, J.H. Ahn, T.W. Lee, Extremely efficient flexible organic light-emitting diodes with modified graphene anode, *Nat. Photonics* 6 (2012) 105–110.
- [17] J.H. Park, W. Jung, D. Cho, J.T. Seo, Y. Moon, S.H. Woo, C. Lee, C.Y. Park, J.R. Ahn, Simple, green, and clean removal of a poly(methyl methacrylate) film on chemical vapor deposited graphene, *Appl. Phys. Lett.* 103 (2013).
- [18] J.W. Suk, W.H. Lee, J. Lee, H. Chou, R.D. Piner, Y.F. Hao, D. Akinwande, R.S. Ruoff, Enhancement of the electrical properties of graphene grown by chemical vapor deposition via controlling the effects of polymer residue, *Nano Lett.* 13 (2013) 1462–1467.
- [19] B.H. Lee, J.H. Lee, Y.H. Kahng, N. Kim, Y.J. Kim, J. Lee, T. Lee, K. Lee, Graphene-conducting polymer hybrid transparent electrodes for efficient organic optoelectronic devices, *Adv. Funct. Mater.* 24 (2014) 1847–1856.
- [20] T. Sun, Z.L. Wang, Z.J. Shi, G.Z. Ran, W.J. Xu, Z.Y. Wang, Y.Z. Li, L. Dai, G.G. Qin, Multilayered graphene used as anode of organic light emitting devices, *Appl. Phys. Lett.* 96 (2010).
- [21] Y.Y. Han, L. Zhang, X.J. Zhang, K.Q. Ruan, L.S. Cui, Y.M. Wang, L.S. Liao, Z.K. Wang, J.S. Jie, Clean surface transfer of graphene films via an effective sandwich method for organic light-emitting diode applications, *J. Mater. Chem. C* 2 (2014) 201–207.
- [22] H. Kim, S.H. Bae, T.H. Han, K.G. Lim, J.H. Ahn, T.W. Lee, Organic solar cells using CVD grown graphene electrodes, *Nanotechnology* 25 (2014).
- [23] P. Lin, W.C.H. Choy, D. Zhang, F.X. Xie, J.Z. Xin, C.W. Leung, Semitransparent organic solar cells with hybrid monolayer graphene/metal grid as top electrodes, *Appl. Phys. Lett.* 102 (2013).
- [24] Y. Wang, S.W. Tong, X.F. Xu, B. Özyilmaz, K.P. Loh, Interface engineering of layer-by-layer stacked graphene anodes for high-performance organic solar cells, *Adv. Mater.* 23 (2011) 1514–1518.
- [25] Y.P. Wu, Y.F. Hao, H.Y. Jeong, Z. Lee, S.S. Chen, W. Jiang, Q.Z. Wu, R.D. Piner, J. Kang, R.S. Ruoff, Crystal structure evolution of individual graphene islands during CVD growth on copper foil, *Adv. Mater.* 25 (2013) 6744–6751.
- [26] P.R. Kidambi, C. Weijtens, J. Robertson, S. Hofmann, J. Meyer, Multifunctional oxides for integrated manufacturing of efficient graphene electrodes for organic electronics, *Appl. Phys. Lett.* 106 (2015).
- [27] H. Park, J.A. Rowehl, K.K. Kim, V. Bulovic, J. Kong, Doped graphene electrodes

- for organic solar cells, *Nanotechnology* 21 (2010).
- [28] A. Kasry, M.A. Kuroda, G.J. Martyna, G.S. Tulevski, A.A. Bol, Chemical doping of large-area stacked graphene films for use as transparent, conducting electrodes, *ACS Nano* 4 (2010) 3839–3844.
- [29] X. Wang, L.J. Zhi, K. Müllen, Transparent, conductive graphene electrodes for dye-sensitized solar cells, *Nano Lett.* 8 (2008) 323–327.
- [30] J. Meyer, P.R. Kidambi, B.C. Bayer, C. Weijtens, A. Kuhn, A. Centeno, A. Pesquera, A. Zurutuza, J. Robertson, S. Hofmann, Metal oxide induced charge transfer doping and band alignment of graphene electrodes for efficient organic light emitting diodes, *Sci. Rep.* 4 (2014).
- [31] S. Sanders, A. Cabrero-Vilatela, P.R. Kidambi, J.A. Alexander-Webber, C. Weijtens, P. Braeuninger-Weimer, A.I. Aria, M.M. Qasim, T.D. Wilkinson, J. Robertson, S. Hofmann, J. Meyer, Engineering high charge transfer n-doping of graphene electrodes and its application to organic electronics, *Nanoscale* 7 (2015) 13135–13142.
- [32] M.H. Griep, E. Sandoz-Rosado, T.M. Tumlin, E. Wetzel, Enhanced graphene mechanical properties through ultrasoft copper growth substrates, *Nano Lett.* 16 (2016) 1657–1662.
- [33] C.F. Chen, C.H. Park, B.W. Boudouris, J. Horng, B. Geng, C. Girit, A. Zettl, M.F. Crommie, R.A. Segalman, S.G. Louie, F. Wang, Controlling inelastic light scattering quantum pathways in graphene, *Nature* 471 (2011) 617–620.
- [34] N. Li, S. Oida, G.S. Tulevski, S.J. Han, J.B. Hannon, D.K. Sadana, T.C. Chen, Efficient and bright organic light-emitting diodes on single-layer graphene electrodes, *Nat. Commun.* 4 (2013).
- [35] Z.C. Li, P. Wu, C.X. Wang, X.D. Fan, W.H. Zhang, X.F. Zhai, C.G. Zeng, Z.Y. Li, J.L. Yang, J.G. Hou, Low-temperature growth of graphene by chemical vapor deposition using solid and liquid carbon sources, *ACS Nano* 5 (2011) 3385–3390.
- [36] A. Pirkle, J. Chan, A. Venugopal, D. Hinojos, C.W. Magnuson, S. McDonnell, L. Colombo, E.M. Vogel, R.S. Ruoff, R.M. Wallace, The effect of chemical residues on the physical and electrical properties of chemical vapor deposited graphene transferred to SiO₂, *Appl. Phys. Lett.* 99 (2011).
- [37] A. Das, S. Pisana, B. Chakraborty, S. Piscanec, S.K. Saha, U.V. Waghmare, K.S. Novoselov, H.R. Krishnamurthy, A.K. Geim, A.C. Ferrari, A.K. Sood, *Nat. Nanotechnol.* 3 (2008) 210–215.
- [38] Z.G. Cheng, Q.Y. Zhou, C.X. Wang, Q. Li, C. Wang, Y. Fang, Toward intrinsic graphene surfaces: a systematic study on thermal annealing and wet-chemical treatment of SiO₂-supported graphene devices, *Nano Lett.* 11 (2011) 767–771.